Cell and Tissue Research (2019) 378:267–277
https://doi.org/10.1007/s00441-019-03077-9

REGULAR ARTICLE

A novel homozygous nonsense mutation in *CAST* associated with PLACK syndrome

Şehime Gülsün Temel[1,2] · B. Karakaş[3] · Ü. Şeker[4] · B. Turkgenç[5] · Ö. Zorlu[4] · H. Sarıcaoğlu[4] · Ç. Oğur[6] · Ö. Kütük[7] · D. P. Kelsell[8] · M. C. Yakıcıer[9]

Received: 18 September 2018 / Accepted: 8 July 2019 / Published online: 7 August 2019

Abstract

Peeling skin syndrome is a heterogeneous group of rare disorders. Peeling skin, leukonychia, acral punctate keratoses, cheilitis and knuckle pads (PLACK syndrome, OMIM616295) is a newly described form of PSS with an autosomal recessive mode of inheritance. We report a 5.5-year-old boy with features of PLACK syndrome. Additionally, he had mild cerebral atrophy and mild muscle involvements. Whole exome sequencing was performed in genomic DNA of this individual and subsequent analysis revealed a homozygous c.544G > T (p.Glu182*) nonsense mutation in the *CAST* gene encoding calpastatin. Sanger sequencing confirmed this variant and demonstrated that his affected aunt was also homozygous. Real-time qRT-PCR and immunoblot analysis showed reduced calpastatin expression in skin fibroblasts derived from both affected individuals compared to heterozygous family members. In vitro calpastatin activity assays also showed decreased activity in affected individuals. This study further supports a key role for calpastatin in the tight regulation of proteolytic pathways within the skin.

Keywords Peeling skin syndrome · PLACK syndrome · Whole exome sequencing · *CAST* gene · Calpastatin

Introduction

Peeling skin syndrome (PSS; OMIM 270300) is characterized by continuous shedding of the stratum corneum of the epidermis accompanied by diverse clinical findings including erythema, vesicular lesions, or other ectodermal features (Kurban and Azar 1969; Levy and Goldsmith 1982; Hashimoto et al. 2000; Judge et al. 2004). It is classified into two clinical forms; either acral PSS (APSS; OMIM 609796) or generalized PSS (GPSS; OMIM 270300) (Bowden 2011). APSS involves mainly skin fragility of the palmar, plantar and dorsal part of hands and feet. Previously, mutations in genes encoding for transglutaminase (*TGM5*) and cysteine protease inhibitor cystatin A (*CSTA*; OMIM 184600), which are known to have

Part of this research was presented as a poster presentation at the American Academy of Dermatology Annual Meeting 2018, San Diego and the abstract was published in the Journal of American Academy Dermatology (JAAD) (2018): Volume 79, Issue 3, Supplement 1, Page AB16, DOI: https://doi.org/10.1016/j.jaad.2018.05.108.

✉ Şehime Gülsün Temel
sehimegtemel@hotmail.com; sehime@uludag.edu.tr

[1] Faculty of Medicine, Department of Medical Genetics, University of Uludag, Bursa, Turkey

[2] Faculty of Medicine, Department of Histology & Embryology, University of Uludag, Bursa, Turkey

[3] Molecular Biology, Genetics and Bioengineering Program, Sabancı University, Istanbul, Turkey

[4] Faculty of Medicine, Department of Dermatology, University of Uludag, Bursa, Turkey

[5] Acıbadem Genetic Diagnosis Center, University of Acıbadem, Istanbul, Turkey

[6] Bahçeci Genetic Diagnosis Center, Altunizade, Istanbul, Turkey

[7] Faculty of Medicine, Department of Medical Genetics, Baskent University, Adana, Turkey

[8] Centre for Cell Biology and Cutaneous Research, The Blizard Institute, Barts and The London School of Medicine and Dentistry, Queen Mary University of London, London E1 2AT, UK

[9] Faculty of Arts and Sciences, Department of Molecular Biology and Genetics, University of Acibadem, Istanbul, Turkey

key roles in cross-linking of cornified cell envelope proteins in epidermis, have been associated with APSS (Cassidy et al. 2005; Kharfi et al. 2009; Krunic et al. 2013). GPSS can present with severe pruritis, atopy, patchy feeling of entire skin, food allergies, repeated episodes of angioedema, urticaria and asthma, which can be further divided into inflammatory or non-inflammatory GPSS. Mutations in corneodesmosin (*CDSN*; OMIM 602593) and *CHST8* (OMIM 610190), encoding N-acetylgalactosamine-4-O-sulfotransferase have been associated with inflammatory GPSS (Oji et al. 2010; Israeli et al. 2011; Cabral et al. 2012).

Recently, a new recessive form of GPSS with peeling skin, leukonychia, acral punctate keratoses, cheilitis and knuckle pads (termed PLACK syndrome) has been described and is associated with the loss of function mutations in the *CAST* gene (OMIM 114090; Refseq NM_001042440.4) encoding calpastatin (Lin et al. 2015; Alkhalifah et al. 2017). To date, homozygous mutations of c.607dupA (p.Ile203Asnfs∗8), c.424A>T (p.Lys142∗) and c.1750delG (p.Val584Trpfs∗37) (Lin et al. 2015) and, recently, a homozygous 4-base insertion c.461dupGCAT (p.Ser154Cysfs*6) (Alkhalifah et al. 2017) have been reported in the *CAST* gene leading to loss of function of calpastatin. The aim of this study is to investigate a family displaying features of PLACK syndrome.

Materials and methods

Cases and clinical data

The proband is a 5.5-year old boy who initially presented with skin fragility to the Department of Dermatology Uludag University, Faculty of Medicine, Bursa, Turkey. Clinical assessment identified fragile skin, wooly hair, sparse eyelashes and brows, palmoplantar punctate keratoderma, follicular hyperkeratosis, knuckle pads and cheilitis. Cerebral atrophy and mild muscle involvement were observed on magnetic resonance imaging (MRI) and nerve conduction velocity (NCV)/electromyography (EMG), respectively. Full neurologic assessment by a pediatric neurologist revealed just a slight activation of the deep tendon reflexes. Family members were recruited to the study and their personal medical history was reviewed and physically examined.

This revealed that the proband's aunt had similar clinical cutaneous features but in milder form with in addition nail dystrophy. Though not evaluated by MRI and NCV/EMG due to pregnancy, his aunt's neurological assessment was normal. Pedigree analysis revealed that the condition was segregating as an autosomal recessive trait. Written informed consent for the study was obtained from all participants and blood was collected from the two affected and five unaffected family members.

The study and data collection were in accordance with the principles of the Declaration of Helsinki and the study had the approval of the local ethical committee.

Whole exome sequencing and sanger sequencing

Genomic DNA was isolated from blood samples using Wizard® Genomic DNA Purification Kit, Promega. Whole exome sequencing (WES) and analysis were performed on 3 samples (proband, father and mother) at the core facility of Advanced Genomics and Bioinformatics Research Center (IGBAM, TUBITAK, Gebze, Turkey) using Illumina technology.

DNA samples were prepared for massively parallel sequencing by using an Illumina TruSeq Sample Preparation kit. Exonic regions were captured by a NimbleGen SeqCap EZ Human Exome Library v3.0 Kit. Illumina TruSeq PE Cluster Kit v3-cBot-HS was used for paired-end cluster generation and a TruSeq SBS Kit v3-HS reagent kit was used for sequencing the post-capture libraries. Initial clustering was performed on an Illumina cBot machine. Paired-end sequencing was done on an Illumina HiSeq 2500 system with a read length of PE 2 × 104. All procedures were carried out according to the manufacturer's instructions. Base calling and image analysis were done using Illumina's Real Time Analysis software version 1.13 with default parameters.

Raw sequencing data were aligned to the hg19 reference human genome using BWA (Li and Durbin 2009) with standard parameters in paired-end (PE) mode. SAMtools (Li et al. 2009) was then used to remove PCR duplicates. To calculate the coverage of targeted exome regions, BEDtools (Quinlan and Hall 2010) was used. To perform local realignment around indels, Genome Analysis Toolkit v1.6 (GATK) (DePristo et al. 2011) IndelRealigner was used. Then, SNPs and small indels were called by using GATK UnifiedGenotyper. SnpEff (Cingolani et al. 2012) was used for functional annotation of variants such as gene/exonic region, minor allele frequency, segmental duplications and effect of variants. HomSI (Görmez et al. 2014) was used for homozygosity mapping analysis. Homozygous candidate variants were sifted using FMFilter (Akgün et al. 2016).

The homozygous rare/novel sequence variants identified in *CAST* and *VPS13C* were verified by Sanger sequencing in family members using the GenomeLab™ GeXP Genetic Analysis System (Beckman Coulter, Germany). DNASTAR sequence analysis software and sub-components were used for sequence assembly and analysis of Sanger data (DNASTAR Inc., USA). CAST sequencing primers, forward 5′ TTTGGTAGCAAGGG AATTGG and reverse 5′ AGATCAGGCTCTGG AAAGCA; and VPS13C sequencing primers, forward 5′

TTAGGGAACAGCAGAAACTCA and reverse 5′ AACATCCCACTTGATTACGC oligonucleotide primers, were used for PCR amplification following DNA sequencing.

Histogical and immunohistochemical analysis

Hematoxyline-eosine staining was applied to the paraffin-embedded skin tissue sections of the proband (III:7). Immunohistochemical staining was performed with a calpastatin antibody (1:100, sc-376547, Santa Cruz Biotechnology, Inc., Santa Cruz, CA) in the paraffin-embedded skin tissue sections of the proband (III:7) and the control of a skin age and sex matched tissue, available in the Pathology Department of Near East University.

Transmission electron microscopy analysis

Briefly, skin tissue was fixed in 2.5% glutaraldehyde solution in PBS (phosphate-buffered saline) (1×, pH 7.4), pH 7.4, for 4 h and post-fixed for 1 h in 1% osmium tetroxide in 0.1 M 1X-PBS. After washing in 1× PBS, they were dehydrated through ethanol series, treated with propylene oxide and embedded in Araldite/Epon812 (Cat. no. 13940, EMS, Hatfield, PA, USA). After heat polymerization, sections were cut using a microtome. Semi-thin sections were stained with methylene blue-azure II and examined using a light microscope (Leica Microsystems, Germany) with a DC490 digital camera (Leica Microsystems, Germany). Ultrathin sections (Leica ultracut R, Germany) were double-stained with uranyl acetate and lead citrate (Leica EM AC20, Germany). These sections were examined in a JEOL-JEM 1400 (Jeol USA Inc) electron

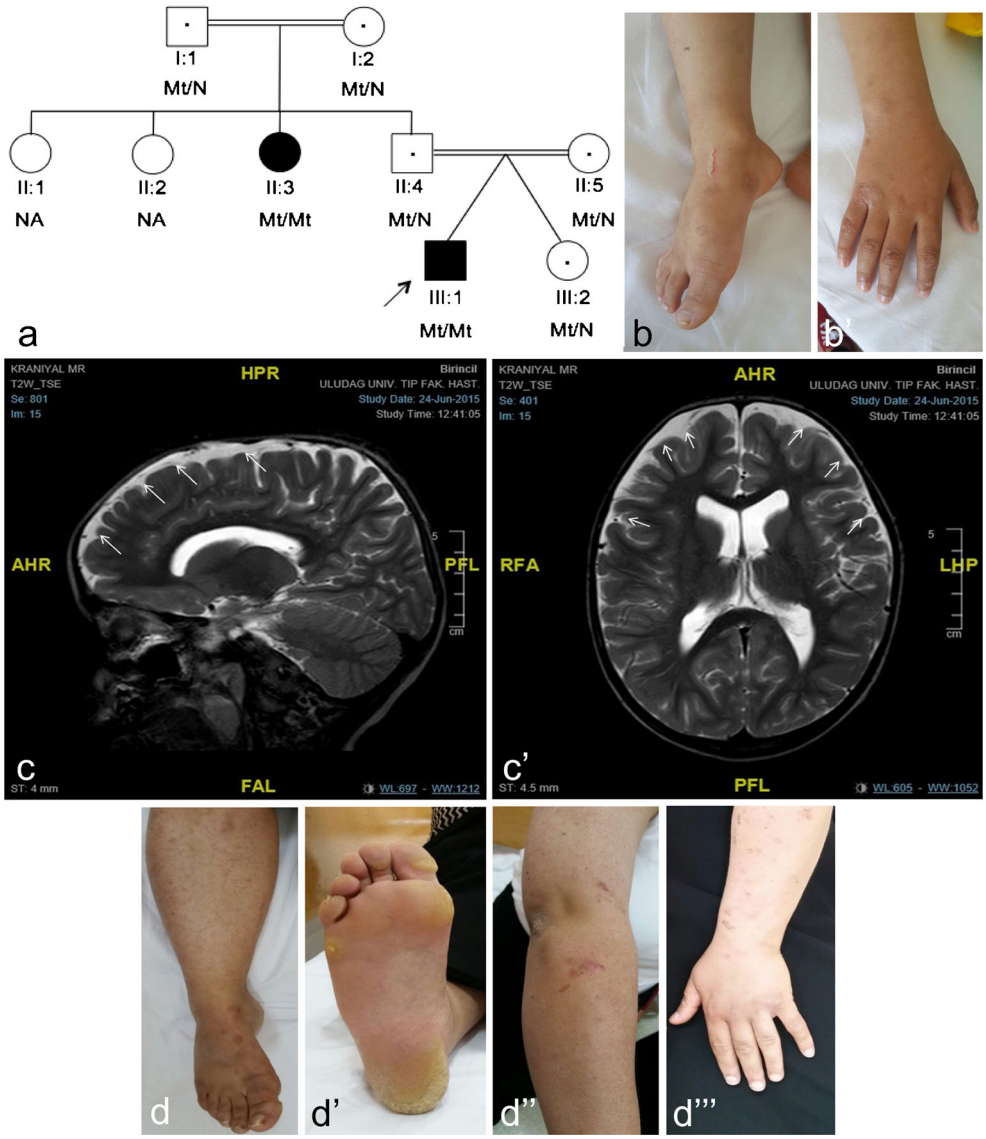

Fig. 1 The PLACK family and clinical features. **a** Pedigree of PLACK family. Parents are first cousins. **b** skin fragility and **b"** knuckle pads. **c** Axial and **c'** sagittal T2-weighted images revealed mild cerebral atrophy and evidence of peripheral CSF areas secondary to atrophy by MRI (indicated by white arrows). **d** Showing the paternal aunt's (II-3) nail dystrophy, **d'** follicular hyperkeratosis **d"** and eroded bullous lesion residuals **d"'** in her arm

microscope and photographed by CCD camera (Gatan Inc., Pleasanton, CA, USA).

Cell culture of human skin fibroblasts

Human skin biopsies were obtained from both affected patients and, initially, washed with 1× PBS and incubated in 37 °C for 60 min. The samples were washed once with 1× PBS, diced and incubated with collagenase type CLS IV (Millipore, Germany) in 37 °C for 120 min under rotation. Samples were then washed in DMEM plus 5% FBS and centrifuged 1200 rpm for 10 min. Cell pellets were then cultured in a 12-well plate in DMEM supplemented with 10% (*v*/*v*) fetal bovine serum (FBS; PAN, Cat. no. P30-3302), antibiotics (penicillin/streptomycin; Biological Industries, Cat. no. 03-031-1B) and 1% (2 mM) L-glutamine (Biological Industries, Cat. no. 03-020-1B).

Real-time qPCR

Total RNA was extracted from cultured fibroblasts using RNeasy kit (Qiagen, USA). To quantify mRNA expression of *CAST* gene, qRT-PCR was carried out using following primers (CASTContF:catgatttctgctggtggag, CASTContR:ccctatgggtttcgaagagtc primer pair that amplify upstream of the variant region, and CASTcE182XF:GGACCAGAAGTTTCAGATCCAA, CASTcE182XR:TCCCTGCTGACTGAGCTTTT primer pair that amplify the region that includes c.544G>T (p.Glu182*)) and 1-step QuantiTect SYBR Green qRT-PCR Kit (Qiagen, USA) according to the manufacturer's standard protocol on Light Cycler 480 instrument (Roche, Switzerland). The housekeeping gene *GAPDH* (Hs_GAPDH_1_SG QuantiTect Primer Assay, NM_002046, Qiagen) was used for normalization, and relative gene expression levels were calculated using the $2^{-\Delta\Delta Ct}$ method. Results are shown as fold expression (mean ± SEM, $n = 3$; bars, SE; $^{*}P < .05$, $^{**}P < .01$). Statistical significance was analyzed by using Student's *t*-tail test on GraphPad Prism 6.2 software.

Immunoblotting

Total cell lysates from fibroblasts were prepared in 1% CHAPS buffer [5 mM $MgCl_2$, 140 mM NaCl, 1 mM EDTA, 1 mM EGTA, 1% CHAPS, 20 mM Tris-HCl (pH 7.5) and protease inhibitors (completeULTRA, Roche)]. Total cell lysates were separated on 12% SDS-PAGE gels. After SDS PAGE, proteins were transferred onto PVDF membranes (Millipore Darmstadt, Germany) and then blocked with 5% dried milk in PBS-Tween 20. Membranes were incubated with primary and secondary antibodies (GE Healthcare) in a buffer containing 10% milk diluent-blocking concentrate (KPL, Sera Care, USA), detected with Luminata Crescendo Western HRP

Table 1 Novel and rare homozygous variants in the exome file of the proband

Chr	Gene	Transcript ID	Variant type	Variant	dbSNP ID	Minor allele frequency (MAF)		Protein predictions			OMIM fenotype	Pathogenic class
						gnomAD exomes	gnomAD genomes	SIFT	Mutation taster	Provean		
chr1	*KHDRBS1*	NM_006559.3	Synonymous	c.1266G>A (p.Ser422=)	rs780046000	0.000016	NA	–	–	–	NA	VUS
chr1	*OLFML2B*	NM_015441.2	Missense	c.1136C>T (p.Ser379Leu)	rs145215702	0.00018	NA	D	P	N	NA	VUS
chr5	*TMCC1*	NM_001017395.4	Synonymous	c.1815C>T (p.Ser605=)	rs775227252	0.000024	NA	–	–	–	NA	VUS
chr5	*CAST*	NM_001284213.3	Nonsense	c.544G>T (p.Glu182*)	NA	NA	NA	–	DC	–	#616295	Pathogenic
chr9	*CCDC183*	NM_001039374.4	Missense	c.223G>A (p.Gly75Arg)	rs771245508	0.000016	NA	T	P	N	NA	VUS
chr11	*GDPD4*	NM_182833.2	Missense	c.400G>C (p.Val134Leu)	rs143423593	0.0043	0.0047	T	P	P	NA	VUS
chr15	*VPS13C*	NM_018080.3	Missense	c.8004G>A (p.Met2668Ile)	rs757188811	0.000012	NA	T	DC	N	#616840	VUS
chr18	*NOL4*	NM_001198548.1	Missense	c.214G>C (p.Gly72Arg)	rs890471029	0.000008	NA	T	DC	N	NA	VUS

KHDRBS1 and *TMCC1* variants were silent substitutions that do not change the encoded amino acid and were not OMIM phenotype

chr chromosome, *D* damaging, *DC* disease causing, *N* neutral, *NA* not available, *P* polymorphism, *T* tolerated, *VUS* variant of unknown significance

substrate (Millipore, Darmstadt, Germany). Blots were imaged with ImageQuant LAS 4000, (Fujitsu/GE Life Science, USA) on chemiluminescence mode. The following antibodies were used for immunoblotting: calpastatin (A-1) (Santa Cruz Biotechnology, CA sc-376547), GAPDH (#2118, Cell Signaling, MA, USA).

Immunofluorescence staining and confocal laser scanning microscopy

Fibroblasts grown on sterile coverslips (Jena Bioscience circular cover slide (22 mm), # CSL-104) were incubated in a 12-well plate format at 37 °C, washed for three times for 5 min per rinse (each wash step are the same unless specified otherwise) with 1× PBS, fixed for 10 min with 4% (*v*/*v*) paraformaldehyde in 1× PBS, followed by rinsing in 1× PBS. Cell membranes were permeabilized by incubation in 0.05% Triton100-X in 1× PBS for 5 min followed by rinsing with 1× PBS. The fixed and permeabilized cells were incubated with 0.1% bovine serum albumin (BSA) in 1× PBS (blocking buffer) for 30 min at room temperature. Coverslips were exposed to primary antibody 1:100 (*v*/*v*) and calpastatin (A-1) (Santa Cruz Biotechnology, sc-376547) in blocking buffer for 1 h at room temperature. After washing steps with 1× PBS, coverslips were incubated in the dark, with Alexa-488 fluorescence tagged secondary antibody (Alexa Fluor 488 anti-mouse IgG, Invitrogen, Cat. no. A11034) in blocking buffer for 1 h at room temperature and subsequently rinsed in washing buffer. Cells incubated without primary antibody (secondary antibody only) were used as a negative control. Cells were mounted with ProLong Antifade kit (Molecular Probes, Eugene, OR, USA) on glass slides (0.17 mm, Thermo Fisher Scientific Inc., USA) and the stained cells were examined by a Zeiss LSM 710 Confocal Microscope. Specimens were observed through an oil immersion × 63 objective. Slides were imaged with a Zeiss LSM710 confocal microscope, excited with 488 nm (for Alexa 488 labeled antibody); light emissions were collected at 530 nm (green immunofluorescence for calpastatin localization) and DAPI (Excitation 405, Emission (blue) 459 nm) simultaneously. Controls were imaged under similar confocal settings. Images were analyzed by using ZEN Lite software (Zeiss, USA).

Calpastatin activity assay

For the calpastatin activity assay, protein concentrations of the fibroblast-derived cell extracts obtained from patients were adjusted to 3 μg/μL. The extracts were heated to 90 °C for 5 min and then centrifuged at 16,000*g* at 4 °C for 20 min. Reactions contained 5 μL of supernatant, 10 nM human erythrocyte calpain 1 (Millipore, USA), 200 μM Suc-Leu-Leu-Val-Tyr-AMC (Abcam, UK) and 195 μL of the homogenization buffer with 5 mM beta-mercaptoethanol. One sample contained no supernatant and was designated as negative control. The reaction was started by adding $CaCl_2$ to a final

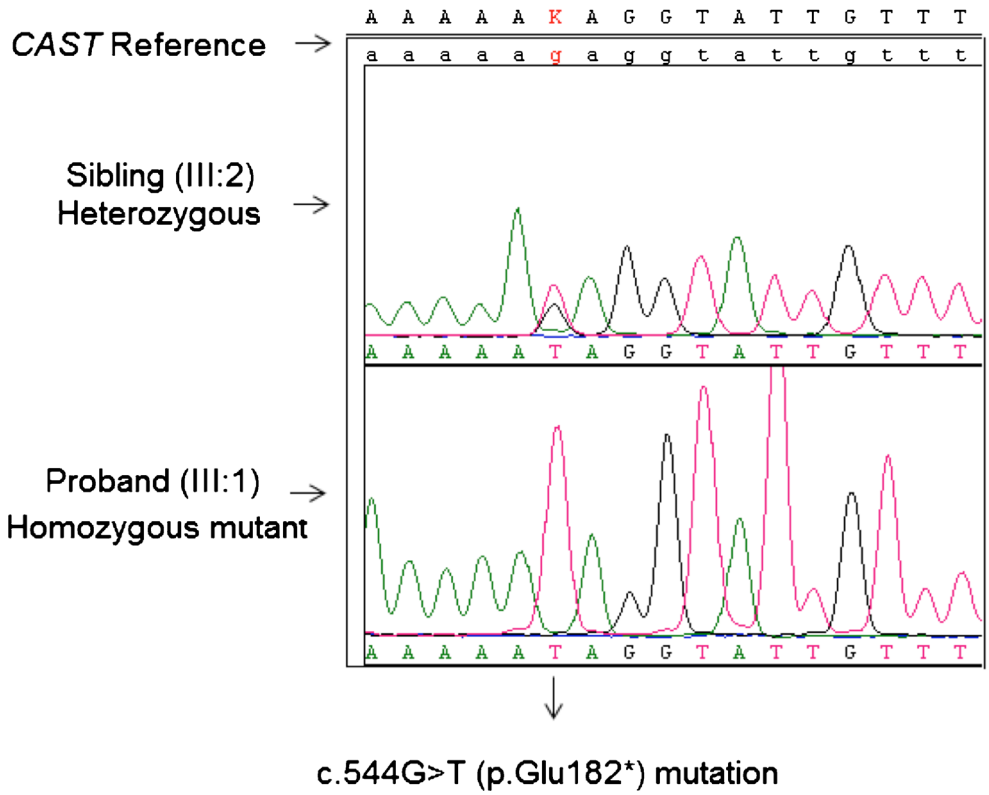

Fig. 2 Mutation detail. Electropherograms for heterozygous and homozygous mutant genotypes of *CAST* c.544G>T (p.Glu182*) nonsense mutation

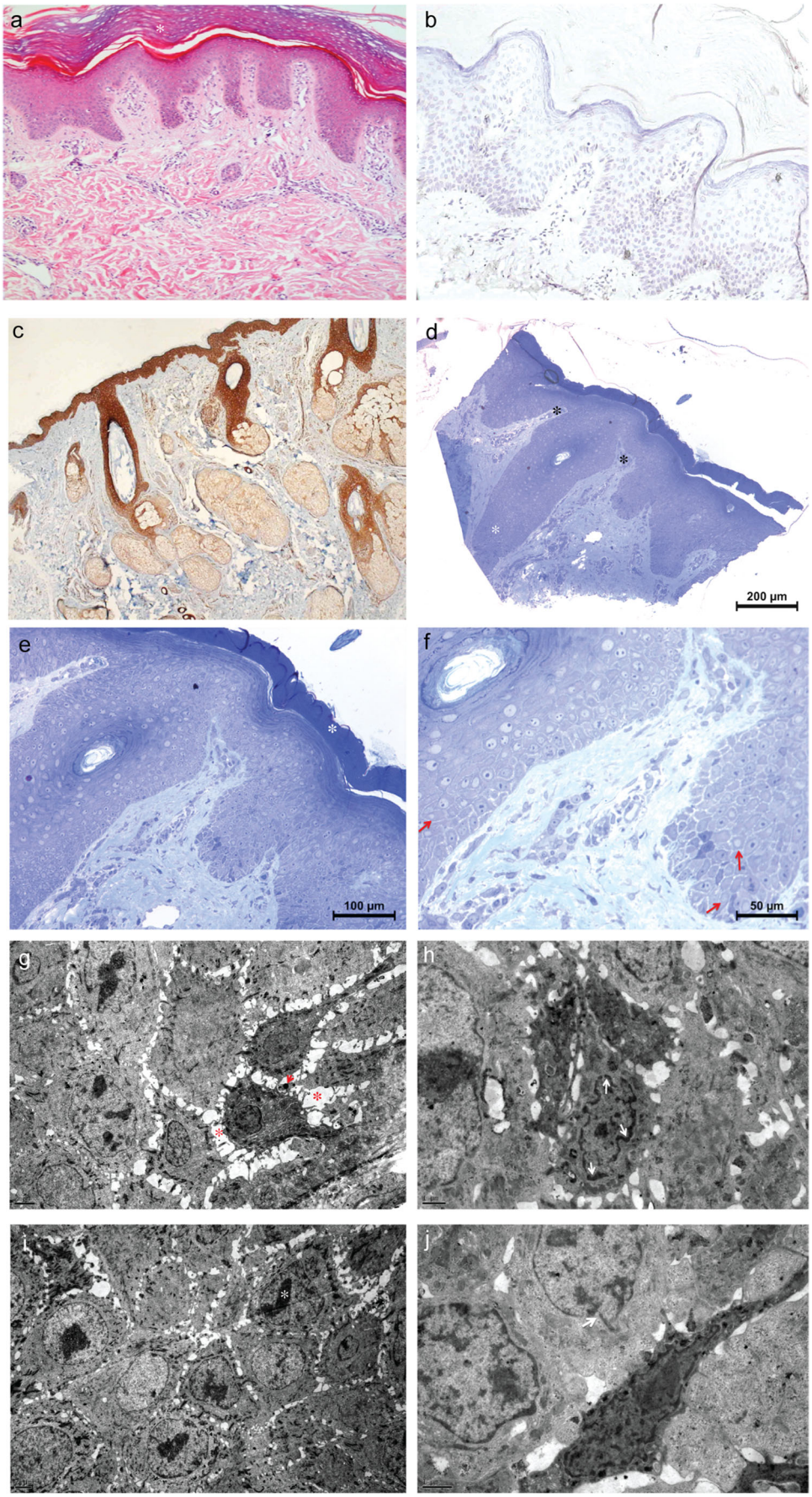
a
b
c
d
200 μm
e
100 μm
f
50 μm
g
h
i
j

◀ **Fig. 3** Histological, immunohistochemical and transmission electron microscopy results. **a** Proband's lesional skin biopsy, photomicrographs showing hyperkeratosis (white asterisk), mild spongiotic changes, H&E. **b**, **c** Immunohistochemistry shows absent calpastatin staining in the proband (**b**) compared to normal staining throughout the epidermis in the control (**c**). **d**–**f** Photomicrographs showing elongated epidermal rete pegs (**d**-white asterisk) and dermal papilla (**d**-black asterisk), thick stratum corneum (**e**-black asterisk), extensive karyolysis even in stratum basale and loss of chromatin pattern in all epithelial cells (**f**-red arrows) and semi-thin sections T&B. **g**–**j** Electron micrographs showing widened intercellular space, heterochromatin in the bleb (**g**-red asterisk, red arrow, respectively), chromatin condensation and marginization (**h**-white arrows), nuclear chromatin condensation and fragmentation (**i**-white asterisk) and the loss of the integrity of the nuclear membrane (**j**-white arrow)

concentration of 5 mM at room temperature. Substrate proteolysis, which results in increasing fluorescence was measured on a fluorescence microplate reader (360 nm excitation, 460 nm emission) at 30 min in triplicate. Data shown are mean relative fluorescence units from three independent experiments; bars, SE; $^{**}P < .01$, $^{**}P < .05$. Statistical significance was analyzed by using Student's *t*-tail test on GraphPad Prism 6.2 software.

Results

Clinical findings

We report on a 5.5-year old boy who initially presented with generalized peeling skin who was the first-born of IVF twins from a consanguineous marriage. Clinical findings included fragile skin (Fig. 1b), wooly hair, sparse eyelashes and brows, palmoplantar punctate keratoderma, follicular hyperkeratosis, knuckle pads (Fig. 1b') and cheilitis. Mild cerebral atrophy, secondarily to atrophy asimetrically enlargement of lateral ventricles and mild muscle involvement were observed on his MRI (Fig. 1c, c') and NCV/EMG, respectively. His aunt also had similar clinical features but in milder form with, in addition, nail dystrophy (Fig. 1d–d'").

WES and sanger sequencing

To search for the putative causative mutation or mutations related with proband's phenotype and presumed autosomal recessive inheritance, we evaluated novel and rare homozygous variants in the exome file and identified eight candidate variants (Table 1). The most plausible variant associated with the cutaneous phenotype segregating in the family was the c.544G>T nonsense variant in *CAST*. However, the pathogenic class of all eight variants was evaluated according to ACMG (American College of Medical Genetics) criteria in company with standards and guidelines for the interpretation of sequence variants (Richards et al. 2015). *KHDRBS1* and *TMCC1* variants were silent substitutions that do not change the encoded amino acid and these genes have not been previously related to any OMIM phenotypes. All of the other five missense variants were predicted as not damaging to protein by at least one of three computational algorithms used. In addition, four of these missense genes, except for *VPS13C*, have not been previously associated with any OMIM phenotypes. The *VPS13C* variant was predicted as not damaging to protein by SIFT and Provean predictions. *VPS13C* mutations have been linked to a form of Parkinson disease (OMIM 616840) but all of the pathogenic variants for the *VPS13C* gene that were reported in HGMD Professional 2018.4 (Human Gene Mutation Database Professional version 2018.4) were truncating or splicing. The parents of the proband (II:4 and II:5), healthy sister (III:2) and grandmother (I:2) were carriers for the *VPS13C* variant and the other affected family member (II-3) had the wild type genotype. She could not be investigated for cerebral atrophy since she was pregnant at that time. Thus, we could not find any strong evidence for the pathogenicity of this homozygous missense *VPS13C* variant found in the proband.

Thus, the remaining *CAST* variant is likely to underlie PLACK syndrome in this family. This homozygous c.544G>T nonsense variant was absent in the following databases: HGMD (Human Gene Mutation Database Professional version 2018-4); ClinVar, CentoMD 5.3, OMIM (Online Mendelian Inheritance In Man); and LOVD v.3.0 (Leiden Open Variation Database version 3.0), as well as in the population specific databases such as dbSNP (Single Nucleotide Polymorphism database), ExAC (Exome Aggregation Consortium), ESP (NHLBI GO Exome Sequencing Project), 1000 Genomes (A Deep Catalog of Human Genetic Variation) TOPMED (NHLBI Trans-Omics for Precision Medicine), and gnomAD (Genome Aggregation Database). Sanger sequencing was used to confirm this variant (Fig. 2) and to show its segregation in the family.

Histological and immunohistochemical findings

H&E staining of proband's lesioned skin showed hyperkeratosis and mild spongiotic changes (Fig. 3a-white asterisk). Immunohistochemistry results showed reduced/absent calpastatin staining in the proband (Fig. 3b) compared to that of control epidermis (Fig. 3c).

Transmission electron microscopy findings

Semi-thin sections of proband's lesioned skin showed elongated epidermal rete pegs (Fig. 3d-white asterisk) and dermal papilla (Fig. 3d-black asterisks), thick stratum corneum (Fig. 3d-white asterisk), extensive karyolysis even in stratum basale and loss of chromatine pattern in all epithelial cells (Fig. 3f-red arrows). Electron micrographs showed widened intercellular

space, heterochromatin in the bleb (Fig. 3g-red asterisk, red arrow, respectively), chromatin condensation and marginization (Fig. 3h-white arrows), nuclear chromatin condensation and fragmentation (Fig. 3i-white asterisk) and the loss of the integrity of the nuclear membrane (Fig. 3j-white arrow).

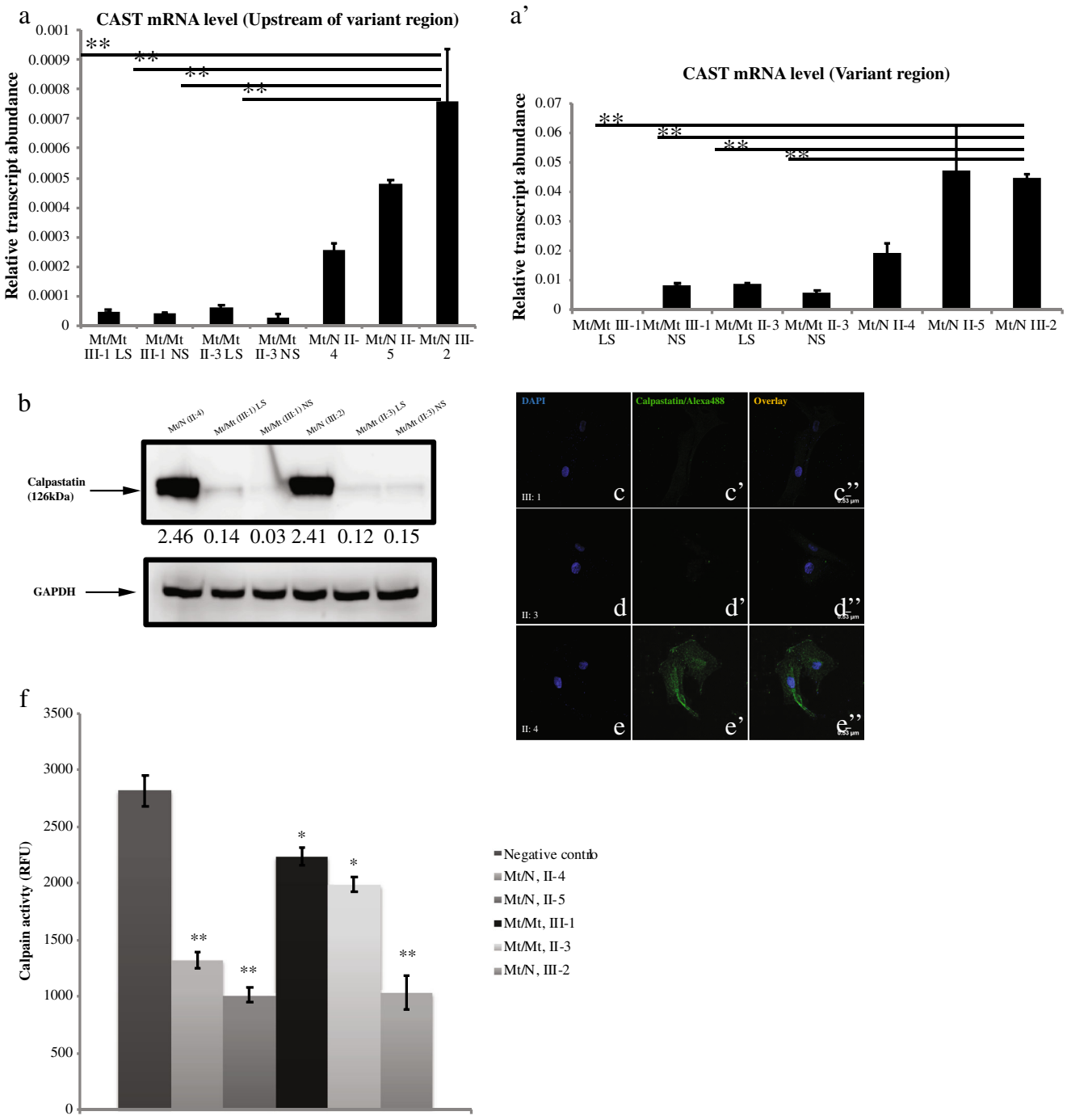

Fig. 4 mRNA quantification results of CAST gene upstream of the variant region (**a**) and the variant region (**a'**), for homozygote (mt/mt) and heterozygote (mt/wt) individuals. The residual expression of CAST mRNA in the affected cases was presented (**b**). Semi-quantitative protein expressions for different genotypes. Calpastatin was normalized to GAPDH, which was set to 1.00 and the intensity ratio of calpastatin to GAPDH was calculated. LS lesioned skin, NS normal skin. Immunofluorescence stainings of CAST for homozygous proband (III-1) (**c**, **c'**, **c"**), for homozygous proband's aunt (II-3) (**d**, **d'**, **d"**) and for heterozygote carrier (III-2) (**e**, **e'**, **e"**). Calpastatin activity assay. Calpastatin activity was indirectly derived from inhibition of calpain activity in protein lysates from homozygote and heterozygote cases. Negative control contains no lysate and indicates baseline calpain activity. Data shown are mean relative fluorescence units from three independent experiments; bars, SE; $^{**}P < .01$, $^{**}P < .05$, affected cases, carriers vs. negative controls (**f**)

Real-time qPCR analysis

In contrast to the carriers, we could detect only trace expression of *CAST* mRNA in the affected cases, probably due to mechanisms of nonsense mediated mRNA decay (Fig. 4a, a'). Furthermore, we demonstrated a significant difference between the expression of mRNA upstream of the variant region and the variant region in affected cases (both Normal Skin (NS) and Lesioned Skin (LS)) and Mt/N III-2. Similarly, we found that expression of *CAST* mRNA was significantly different in affected cases compared to Mt/N II-4 (*$P < .05$) and Mt/N II-5 (**$P < .01$).

Protein quantification and immunofluorescence

To compare the abundance of calpastatin in fibroblasts of individuals with homozygous and heterozygous genotypes, total protein samples were resolved on SDS-PAGE and immunoblotted using calpastatin and GAPDH-specific antibodies. A semi-quantitative protein expression assay revealed a drastically low amount of calpastatin in patients' normal and lesioned skin cells as compared to cells from the heterozygous unaffected cell line (Fig. 4b). Hence, we detected more than a two-fold decrease in calpastatin expression levels in the patients homozygous for c.544G>T (Mt/Mt III:1 and Mt/Mt II:3) compared with heterozygous carriers (Mt/N II:4 and Mt/N III:2). Confocal microscopy results also confirmed reduced expression pattern of calpastatin in fibroblasts from affected patients compared to carriers (Fig. 4c–c", d–d", e–e").

In vitro calpastatin assay findings

In vitro calpastatin activity of fibroblast cell extracts obtained from patients homozygous for c.544G>T (III:1 and II:3) and unaffected heterozygote cases were evaluated indirectly by fluorogenic calpain proteolysis assay using a Suc-Leu-Leu-Val-Tyr-AMC fluorescence probe. Our results demonstrated increased calpain activity and, thus, decreased calpastatin activity in affected individuals compared with control samples (**$P < .01$) (Fig. 4f).

Discussion

PLACK syndrome has recently been described as a new form of peeling skin syndrome (PSS), characterized by generalized peeling skin, leukonychia, acral punctate keratoses, cheilitis and knuckle pads (Lin et al. 2015). To date, four homozygous pathogenic variants (loss of function mutations) in *CAST* gene (c.424A>T, c.607dup, c.1750delG, c.461dupGCAT) have been reported with PLACK syndrome (Lin et al. 2015; Alkhalifah et al. 2017). This study presents the fifth family with PLACK syndrome and is associated with a novel homozygous nonsense mutation (c.544G>T p.Glu182*) in the *CAST* gene.

CAST encodes calpastatin, which is an endogenous specific inhibitor of calpain, a calcium-dependent cysteine protease (Goll et al. 2003). Calpastatin can bind to calcium activated calpains (Potz et al. 2016). Calpains are involved in a range of cellular processes, including cell proliferation (Kovács and Su 2014), migration (Franco and Huttenlocher 2005), wound healing (Nassar et al. 2012), apoptosis and survival (Tan et al. 2006). It is also involved in the regulation of epidermal cell differentiation (Carragher and Frame 2004). A proposed mechanism underlying PLACK syndrome is that the absence of a functional calpastatin prevents the inhibition of calpains leading to elevated keratinocyte apoptosis and skin hyperkeratosis (Lin et al. 2015; Wang et al. 2015).

Modulation of calpastatin expression in mice caused no phenotypic abnormalities under normal conditions indicating that calpastatin may only function as a negative regulator of calpain only under pathological conditions (Takano et al. 2005). In order to determine the functional consequences of *CAST* mutations in vitro, Lin et al. performed siRNA-mediated knockdown of *CAST* in the immortalized keratinocyte cell line, HaCaT and performed a mechanical induced stress assay. This showed that mechanical stress revealed breakage of the intercellular connections in *CAST* knock down cell monolayers in contrast to control cell lines (Lin et al. 2015). Calpain overactivity is involved in the pathophysiology of a large number of disease processes of the brain, eyes, heart, lungs, pancreas, kidneys, vascular system and skeletal muscle. The situation of stress leads to increased calcium ion release causing over-activation of calpain, which may cause organ dysfunction by promoting cellular apoptosis and degradation of cytoskeletal structure (Potz et al. 2016). Therefore, calpain was suggested as a potential therapeutic target for a wide variety of disease processes. In line with this, inhibition of calpain by over-expression of calpastatin inhibits the abnormal breakdown of cytoskeletal proteins (spectrin, MAP2 and neurofilaments) and ameliorates motor axon loss in amyotrophic lateral sclerosis (ALS) hSOD1G93A transgenic mouse model (Rao et al. 2016). Another study supports the hypothesis that calpastatin may play a role in regulating the initial metastatic dissemination of breast cancer (Storr et al. 2011).

It is noteworthy that our novel mutation and the associated clinical features differ in that leukonychia was absent although it was reported in all of the previous cases. Mild cerebral atrophy and muscle involvement was also present in one of the affected family members, whereas it was not reported in the study by Lin et al. (2015). However, Alkhalifah et al. (2017) did report muscle involvement in their study. The absence of leukonychia and the presence of mild cerebral atrophy in our patient suggest significant phenotypical variability within individuals with *CAST* mutations.

In this study, we demonstrated that calpastatin expression in fibroblasts from affected family members was reduced at both the mRNA and protein level. In vitro calpastatin activity revealed reduced calpain proteolysis in both affected individuals. The molecular and biochemical studies in conjunction with the described clinical features in this study emphasize the importance of tight regulation of proteolytic pathways by calpastatin in maintaining the structural integrity of the skin.

Acknowledgments The authors wish to express their gratitude to the family members for participating in this study and Prof. Dr. Esin ASAN for her valuable comments on semithin sections and electronmicrographs and TUBITAK-IGBAM for exome sequencing and bioinformatic advice.

Funding This work was supported by the Uludag University Scientific Research Unit with Project number KUAP(T)-2014/36.

Compliance with ethical standards

Conflict of interest The authors declare that they have no conflict of interest.

Ethical approval All procedures performed in studies involving human participants were in accordance with the ethical standards of the institutional research committee and with the 1964 Helsinki declaration and its later amendments or comparable ethical standards.

Informed consent Informed consent was obtained from all individual participants included in the study. Additional informed consent was obtained from all individual participants and their guardians for whom identifying information is included in this article.

References

Akgün M, Faruk Gerdan Ö, Görmez Z, Demirci H (2016) FMFilter: a fast model based variant filtering tool. J Biomed Inform 60:319–327

Alkhalifah A, Chiaverini C, Del Giudice P, Supsrisunjai C, Hsu CK, Liu L, Charlesworth A, McGrath JA, Lacour JP (2017) PLACK syndrome resulting from a new homozygous insertion mutation in CAST. J Dermatol Sci 88:256–258

Bowden PE (2011) Peeling skin syndrome: genetic defects in late terminal differentiation of the epidermis. J Invest Dermatol 131:561–564

Cabral RM, Kurban M, Wajid M, Shimomura Y, Petukhova L, Christiano AM (2012) Whole-exome sequencing in a single proband reveals a mutation in the CHST8 gene in autosomal recessive peeling skin syndrome. Genomics 99:202–208

Carragher NO, Frame MC (2004) Focal adhesion and actin dynamics: a place where kinases and proteases meet to promote invasion. Trends Cell Biol 14:241–249

Cassidy AJ, van Steensel MA, Steijlen PM, van Geel M, van der Velden J, Morley SM, Terrinoni A, Melino G, Candi E, McLean WH (2005) A homozygous missense mutation in TGM5 abolishes epidermal transglutaminase 5 activity and causes Acral peeling skin syndrome. Am J Hum Genet 77:909–917

Cingolani P, Platts A, Wang le L, Coon M, Nguyen T, Wang L, Land SJ, Lu X, Ruden DM (2012) A program for annotating and predicting the effects of single nucleotide polymorphisms, SnpEff: SNPs in the genome of Drosophila melanogaster strain w1118; iso-2; iso-3. Fly (Austin) 6:80–92

DePristo MA, Banks E, Poplin R, Garimella KV, Maguire JR, Hartl C, Philippakis AA, del Angel G, Rivas MA, Hanna M, McKenna A, Fennell TJ, Kernytsky AM, Sivachenko AY, Cibulskis K, Gabriel SB, Altshuler D, Daly MJ (2011) A framework for variation discovery and genotyping using next-generation DNA sequencing data. Nat Genet 43:491–498

Goll DE, Thompson VF, Li H, Wei W, Cong J (2003) The calpain system. Physiol Rev 83:731–801

Görmez Z, Bakir-Gungor B, Sagiroglu MS (2014) HomSI: a homozygous stretch identifier from next-generation sequencing data. Bioinformatics 30:445–447

Franco SJ, Huttenlocher A (2005) Regulating cell migration: calpains make the cut. J Cell Sci 118:3829–3838

Hashimoto K, Hamzavi I, Tanaka K, Shwayder T (2000) Acral peeling skin syndrome. J Am Acad Dermatol 43:1112–1119

Israeli S, Zamir H, Sarig O, Bergman R, Sprecher E (2011) Inflammatory peeling skin syndrome caused by a mutation in CDSN encoding corneodesmosin. J Invest Dermatol 131:779–781

Judge MR, McLean WHI, Munro CS (2004) Disorders of keratinization. In: Rook's textbook of dermatology (Burns T, Breathnach S, Cox C, Griffiths C eds), vol 2. Blackwell Scientific, Oxford, pp 54–56

Kharfi M, El Fekih N, Ammar D, Jaafoura H, Schwonbeck S, van Steensel MA, Fazaa B, Kamoun MR, Fischer J (2009) A missense mutation in TGM5 causes acral peeling skin syndrome in a Tunisian family. J Invest Dermatol 129:2512–2515

Kovács L, Su Y (2014) The critical role of calpain in cell proliferations. J Biomol Res Ther 3:112

Kurban AK, Azar HA (1969) Familial continual skin peeling. Br J Dermatol 81:191–195

Krunic AL, Stone KL, Simpson MA, McGrath JA (2013) Acral peeling skin syndrome resulting from a homozygous nonsense mutation in the CSTA gene encoding cystatin A. Pediatr Dermatol 30:e87–e88

Levy SB, Goldsmith LA (1982) The peeling skin syndrome. J Am Acad Dermatol 7:606–613

Li H, Durbin R (2009) Fast and accurate short read alignment with Burrows-Wheeler transform. Bioinformatics 25:1754–1760

Li H, Handsaker B, Wysoker A, Fennell T, Ruan J, Homer N, Marth G, Abecasis G, Durbin R, 1000 Genome Project Data Processing Subgroup (2009) 1000 genome project data processing subgroup. The Sequence Alignment/Map format and SAMtools. Bioinformatics 25:2078–2079

Lin Z, Zhao J, Nitoiu D, Scott CA, Plagnol V, Smith FJ, Wilson NJ, Cole C, Schwartz ME, McLean WH, Wang H, Feng C, Duo L, Zhou EY, Ren Y, Dai L, Chen Y, Zhang J, Xu X, O'Toole EA, Kelsell DP, Yang Y (2015) Loss-of-function mutations in CAST cause peeling skin, leukonychia, acral punctate keratoses, cheilitis, and knuckle pads. Am J Hum Genet 96:440–447

Nassar D, Letavernier E, Baud L, Aractingi S, Khosrotehrani K (2012) Calpain activity is essential in skin wound healing and contributes to scar formation. PLoS One 7:e37084

Oji V, Eckl KM, Aufenvenne K, Nätebus M, Tarinski T, Ackermann K, Seller N, Metze D, Nürnberg G, Fölster-Holst R, Schäfer-Korting M, Hausser I, Traupe H, Hennies HC (2010) Loss of corneodesmosin leads to severe skin barrier defect, pruritus, and atopy: unravelling the peeling skin disease. Am J Hum Genet 87:274–281

Potz BA, Abid MR, Sellke FW (2016) Role of calpain in pathogenesis of human disease processes. J Nat Sci 2: pii: e218

Quinlan AR, Hall IM (2010) BEDTools: a flexible suite of utilities for comparing genomic features. Bioinformatics 226:841–842

Rao MV, Campbell J, Palaniappan A, Kumar A, Nixon RA (2016) Calpastatin inhibits motor neuron death and increases survival of hSOD1(G93A) mice. J Neurochem 137:253–265

Richards S, Aziz N, Bale S, Bick D, Das S, Gastier-Foster J, Grody WW, Hegde M, Lyon E, Spector E, Voelkerding K, Rehm HL, ACMG Laboratory Quality Assurance Committee (2015) Standards and

guidelines for the interpretation of sequence variants: a joint consensus recommendation of the American College of Medical Genetics and Genomics and the Association for Molecular Pathology. Genet Med 17:405–424

Storr SJ, Mohammed RA, Woolston CM, Green AR, Parr T, Spiteri I, Caldas C, Ball GR, Ellis IO, Martin SG (2011) Calpastatin is associated with lymphovascular invasion in breast cancer. Breast 20: 413–418

Takano J, Tomioka M, Tsubuki S, Higuchi M, Iwata N, Itohara S, Maki M, Saido TC (2005) Calpain mediates excitotoxic DNA fragmentation via mitochondrial pathways in adult brains: evidence from calpastatin mutant mice. J Biol Chem 280:16175–16184

Tan Y, Wu C, De Veyra T, Greer PA (2006) Ubiquitous calpains promote both apoptosis and survival signals in response to different cell death stimuli. J Biol Chem 281:17689–17698

Wang H, Cao X, Lin Z, Lee M, Jia X, Ren Y, Dai L, Guan L, Zhang J, Lin X, Zhang J, Chen Q, Feng C, Zhou EY, Yin J, Xu G, Yang Y (2015) Exome sequencing reveals mutation in GJA1 as a cause of keratoderma-hypotrichosis-leukonychia totalis syndrome. Hum Mol Genet 24:243–250

The list of public and restricted databases

100 Genomes (A Deep Catalog of Human Genetic Variation): available at http://phase3browser.1000genomes.org/index.html) (last accessed 25 January 2019)

ClinVar: available at https://www.ncbi.nlm.nih.gov/clinvar (last accessed 25 Januaryr 2019)

CentoMD 5.3: available at (https://www.centomd.com) (last accessed 25 January 2019)

dbSNP (Single Nucleotide Polymorphism database): available at https://www.ncbi.nlm.nih.gov/snp) (last accessed 25 January 2019)

ExAC (Exome Aggregation Consortium): available at http://exac.broadinstitute.org) (last accessed 25 January 2019)

ESP (NHLBI GO Exome Sequencing Project): available at http://evs.gs.washington.edu/EVS) (last accessed 25 January 2019)

gnomAD (Genome Aggregation Database): available at http://gnomad.broadinstitute.org/ (last accessed 25 January 2019)

HGMD (Human Gene Mutation Database) Professional version 2018.4: available at https://portal.biobase-international.com/hgmd/pro/start.php (last accessed 25 January 2019)

LOVD v.3.0 (Leiden Open Variantion Database version 3.0): available at http://www.lovd.nl/3.0/home (last accessed 25 January 2019)

OMIM (Online Mendelian Inheritance In Man): available at https://www.omim.org (last accessed 25 January 2019)

TOPMED (NHLBI Trans-Omics for Precision Medicine): available at http://www.nhlbiwgs.org) (last accessed 25 January 2019)

UCSC Genome Browser: available at www.genome.ucsc.edu) (last accessed 25 January 2019)